

## Kuroshio Path Variations South of Japan: Bimodality as a Self-Sustained Internal Oscillation

BO QIU AND WEIFENG MIAO

*Department of Oceanography, University of Hawaii at Manoa, Honolulu, Hawaii*

(Manuscript received 29 January 1999, in final form 15 October 1999)

### ABSTRACT

In the two decades following 1975, the Kuroshio path south of Japan was observed to oscillate interannually between a straight path state and a meandering state. This bimodal condition is in sharp contrast to the decade prior to 1975 when the Kuroshio remained consistently in the straight path state. In situ observations in the upstream East China Sea indicate no obvious correspondence between the magnitude (or the temporal change) of the inflow transport and the Kuroshio path, suggesting the Kuroshio's path alternations in the recent two decades may not be externally determined by the upstream inflow. Using a two-layer primitive-equation model of the North Pacific driven by observed climatological surface wind data, the authors propose that the Kuroshio path oscillation since 1975 can be explained by a self-sustained internal mechanism of the Kuroshio current system. The proposed self-sustained oscillation is maintained by the accumulation of the low potential vorticity (PV) water carried northward by the upstream Kuroshio. This accumulation of the low-PV anomalies strengthens the Kuroshio's southern recirculation gyre and presses the Kuroshio to flow along the coast. The strengthening of the southern recirculation gyre increases the velocity shear of the straight-pathed Kuroshio and leads eventually to the meander path development due to baroclinic/barotropic instability of the system. As the meander of the Kuroshio path grows, detachment of cyclonic eddies mixes coastal-origin, high-PV water offshoreward, weakening, as a result, the recirculation gyre. The above cycle will restart after the low-PV water is replenished from the south and the recirculation gyre spins up again. For the past two decades, this internal oscillation has been operative because the upstream inflow is relatively large due to the decadal increase in the wind-driven Sverdrup transport. In the decade before 1975 when the upstream inflow was small, the internal oscillation would cease because the dissipative forces are able to remove the southern-origin low-PV anomalies without resorting to instability and the meander development.

### 1. Introduction

The Kuroshio and its extension in the northwestern corner of the subtropical North Pacific is one of the oceanic regions where the largest eddy variability is observed. This was realized in many studies of ocean variability based on in situ observations (e.g., Wyrtki et al. 1976) and, more recently, from satellite altimetric measurements. From the viewpoint of large-scale ocean circulation, the high eddy variability in the Kuroshio region is expected. Being a return flow compensating for the wind-driven subtropical interior circulation, the Kuroshio originates at a southern latitude ( $\sim 15^{\circ}\text{N}$ ; see Fig. 1) where the ambient potential vorticity (PV) is relatively low. For the Kuroshio to smoothly rejoin the Sverdrup interior flow at the higher latitude of  $30^{\circ}$ – $35^{\circ}\text{N}$ , the anomalously low PV acquired by the Kuroshio in the south has to be removed by either dissipative and/

or nonlinear forces along its western boundary path. For a narrow boundary current such as the Kuroshio, scaling analyses show that the dissipative force alone is not sufficient to remove the low PV anomalies (Pedlosky 1987; Cessi et al. 1990). The consequence of the Kuroshio's inability to effectively diffuse the PV anomalies along its path is the accumulation of the low PV water in the northwestern corner of the subtropical gyre, which generates a mean anticyclonic recirculation gyre and provides an energy source for flow instability.

That the recirculation gyre is an inseparable part of the Kuroshio system is well demonstrated by lowered acoustic Doppler current profiler (ADCP) measurements from a recent WOCE cruise across the Kuroshio southeast of Japan (see line P10 in Fig. 1). Figure 2, adapted from Firing (1998), shows the surface-to-bottom profile of the eastward velocity from this WOCE cruise. The volume transport of the eastward-flowing Kuroshio, that is, the unshaded area shown in Fig. 2, is 130 Sv (Wijffels et al. 1998:  $\text{Sv} \equiv 10^6 \text{ m}^3 \text{ s}^{-1}$ ). Compared to the maximum Sverdrup transport of about 50 Sv in the subtropical North Pacific (Hautala et al. 1994), this eastward transport of the Kuroshio is more than twice as

---

*Corresponding author address:* Dr. Bo Qiu, Department of Oceanography, University of Hawaii at Manoa, 1000 Pope Road, Honolulu, HI 96822  
E-mail: bo@soest.hawaii.edu

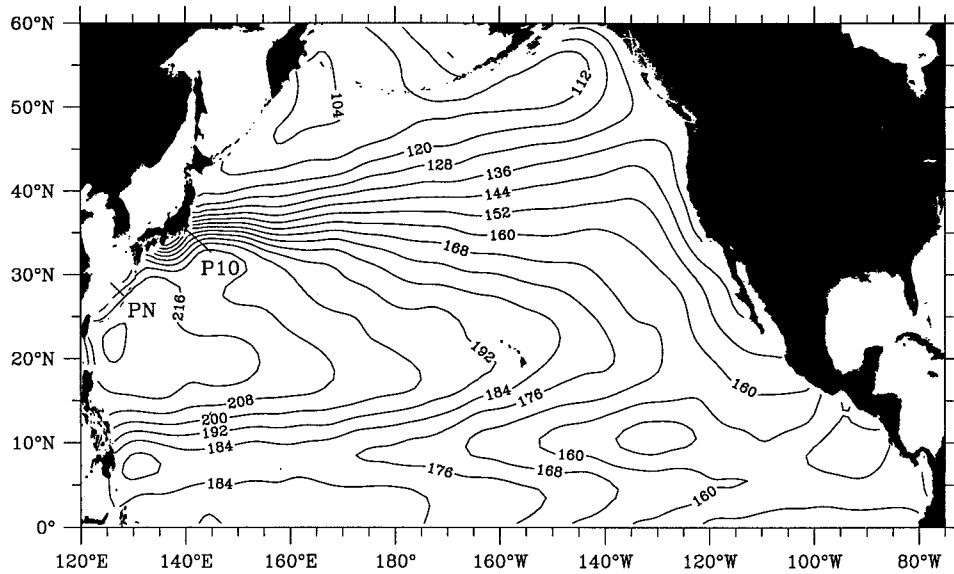


FIG. 1. Mean sea surface dynamic topography relative to 1000 dbar. Units are centimeters. Based on the climatological data sets of Levitus and Boyer (1994) and Levitus et al. (1994). Line P10 denotes the lowered ADCP section of the WOCE P10 cruise. Line PN denotes the repeat hydrographic section in the East China Sea by Japan Meteorological Agency.

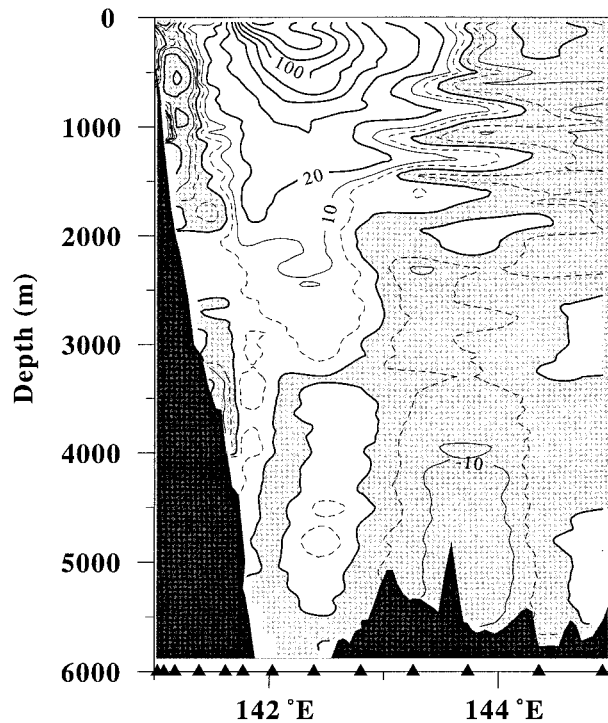


FIG. 2. Eastward velocity profile from lowered ADCP measurements on the WOCE P10 line southeast of Japan in Nov 1993 (see Fig. 1). Units are centimeters per second and westward flow is shaded. Adapted from Firing (1998).

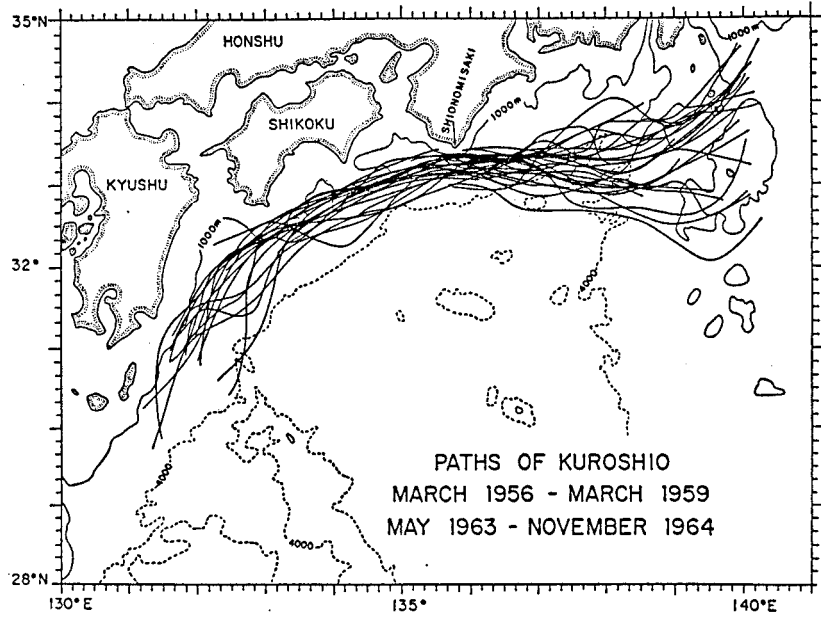
large. Notice that this large eastward transport is due to the presence of the westward recirculating flow south of the Kuroshio, also known as the Kuroshio Counter-current. Though weak in its surface speed, the lowered ADCP measurements show that this westward recirculating flow has a strong barotropic component and has a total volume transport reaching 80 Sv. Clearly, a better understanding of the Kuroshio variability requires knowledge of this recirculating component of the Kuroshio system.

On the interannual timescale, the well-known Kuroshio variability south of Japan is its bimodal path fluctuations. Figure 3, adapted from Taft (1972), is a classical picture depicting the Kuroshio bimodal path patterns. The straight path in the upper panel of Fig. 3 denotes when the Kuroshio flows closely along the Japan coast and the meander path in the lower panel of Fig. 3 signifies when the Kuroshio takes a detouring offshore path. Once formed, both the straight and meander paths can persist over a period ranging from a few years to a decade. In contrast, the transition between the two paths is rapid, often taking place over a period of several months (e.g., Kawabe 1986).

Notice that in addition to this dichotomous view of the Kuroshio path changes, several authors have argued that the Kuroshio south of Japan may take additional, relatively stable paths; one such example is when the Kuroshio path loops southward over the Izu Ridge (near 140°E) rather than being confined to the west of the Izu Ridge as depicted in Fig. 3b. For details, see Kawabe (1985) and Shoji (1972).

As a meandering path of the Kuroshio can vary spatially, one way of indexing the Kuroshio path fluctua-

(a) Straight paths of Kuroshio



(b) Meander paths of Kuroshio

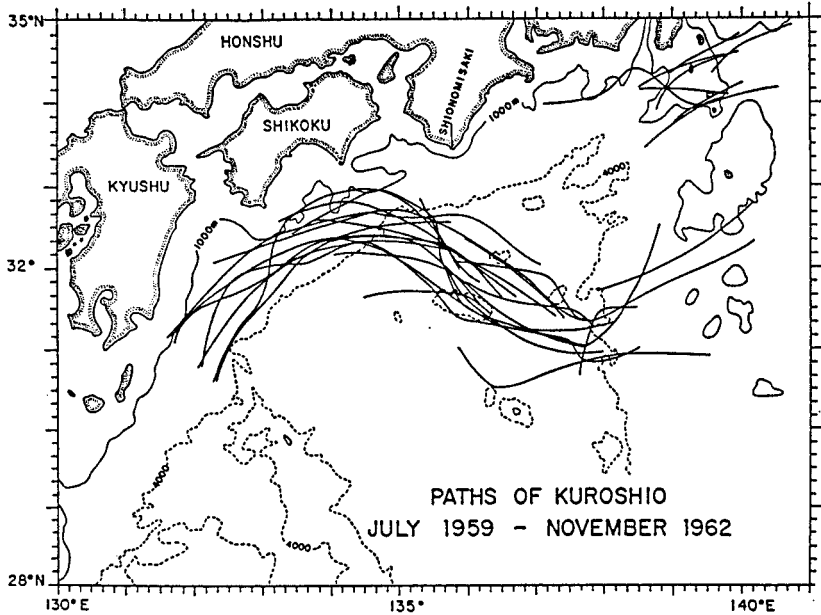


FIG. 3. Examples of the bimodal Kuroshio paths south of Japan. Adapted from Taft (1972).

tions is to use the mean distance of the Kuroshio axis from the Japan coast averaged from 132° to 140°E. A statistical data analysis by Kawai (1969) shows that the 16°C isotherm at the 200-m depth represents well the Kuroshio axis south of Japan. Using all available pub-

lications by Japan Maritime Safety Agency (1955–79, 1977–85, 1986–92, 1993–97) and using Kawai’s indicative for the Kuroshio axis, we plot in Fig. 4a the time series of the Kuroshio path index over the past 42 years. The solid dots in Fig. 4a indicate the seasonally aver-

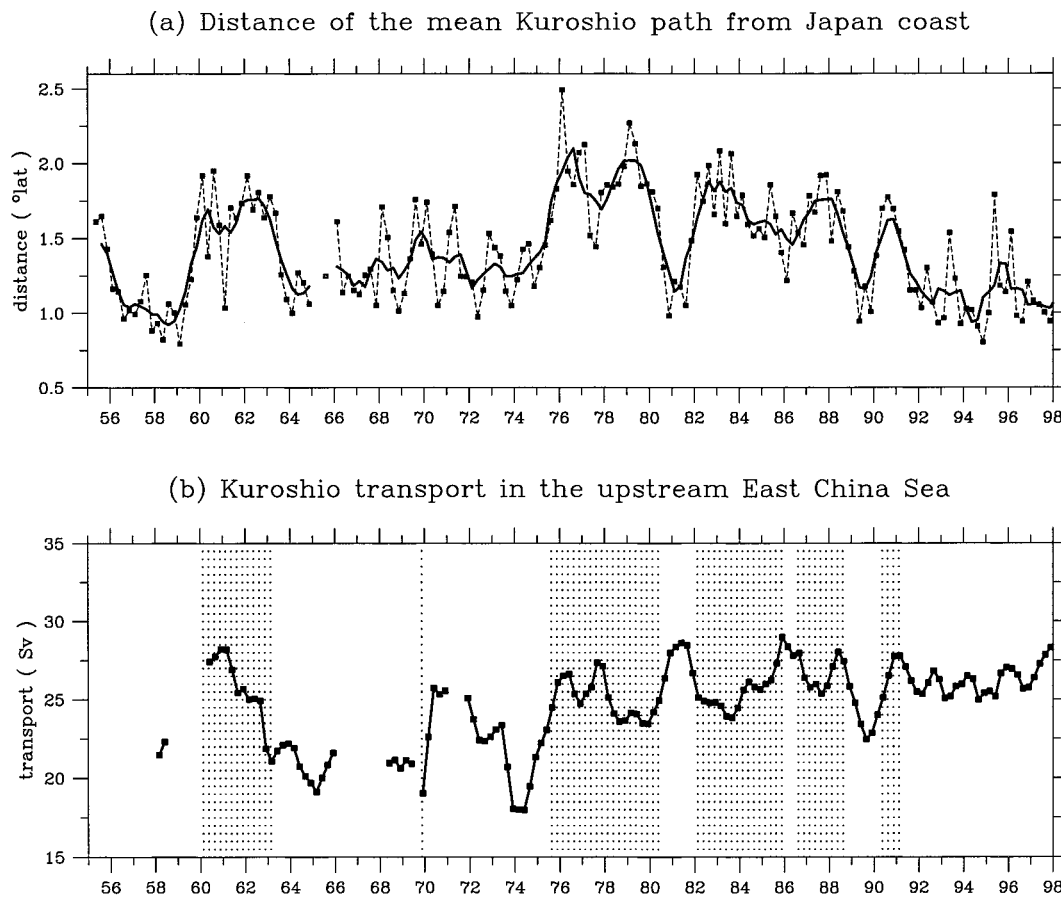


FIG. 4. (a) Time series of the Kuroshio path index from 1955 to 1997. The Kuroshio path index is defined as the offshore distance of the Kuroshio axis (inferred from the  $16^{\circ}\text{C}$  isotherm at the 200-m depth) averaged from  $132^{\circ}$  to  $140^{\circ}\text{E}$ . Closed dots denote the seasonal index values and the solid line indicates the annual average. Data sources for the path index are based on temperature maps published by Japan Marine Safety Agency (1955–97). (b) Time series of the Kuroshio transport along the PN line in the East China Sea. The transport values have been low-pass filtered by the one-year running mean averaging. Data provided by M. Kawabe (1998, personal communication). Shaded areas indicate the large meander periods when the Kuroshio path index exceeds  $1.5^{\circ}$ . Tick marks along the time axes indicate the beginning of a year.

aged index values and the thick line connects the annually averaged indices. A low index in Fig. 4a denotes a straight path of the Kuroshio and a high index denotes an offshore meandering path of the Kuroshio.

The observed Kuroshio path variations, especially the large meander events of 1959–62 and 1975–79, have motivated many data analysis and modeling studies. An early and influential study was that of Nitani (1975) who analyzed repeat hydrographic data across the Kuroshio in the region of  $137^{\circ}$ – $139^{\circ}\text{E}$  and found that the large meander of 1959–62 took place when the Kuroshio had a low eastward transport. Nitani's analysis inspired the early modeling studies by White and McCreary (1976), Chao and McCreary (1982), and Yasuda et al. (1985). In all these modeling studies, the coast of Japan, that is, the northern boundary in their respective inflow–outflow models, was considered to be *zonal*. The Kuroshio was shown to take a meander (straight) path when the inflow transport of the Kuroshio was set to

be small (large); the meandering path was interpreted dynamically as a stationary Rossby lee wave generated by Kyushu Island. In the parameter space of intermediate inflow transport, both Chao and McCreary (1982) and Yasuda et al. (1985) found multiple equilibrium states in which the meandering path and the straight path coexist. The selection between the two paths was shown to be dependent on the time history in the inflow transport change (also see Masuda 1982).

Because of the presence of recirculating westward flows flanking the Kuroshio, it became clear later on that Nitani's calculated Kuroshio transport in the downstream region of  $137^{\circ}$ – $139^{\circ}\text{E}$  may not reflect the true inflow transport of the Kuroshio. Analyses of the sea level data across Tokara Strait by Kawabe (1980) and the geostrophic transport of the Kuroshio in the East China Sea by Saiki (1982) reveal that the upstream Kuroshio transport during the 1959–62 and 1975–79 meander events was, in fact, greater than that in the

straight-path years. These data analysis results reversed the outcomes of more recent modeling studies on the Kuroshio path bimodality. By incorporating into the models the realistic inclination of the Japan coast ( $\sim 20^\circ$  to the due east), all of the recent studies demonstrate that the Kuroshio takes a meander path when the upstream inflow transport  $V_o$  is large and a straight path when  $V_o$  is small (Chao 1984; Yoon and Yasuda 1987; Yamagata and Umatani 1989; Sekine 1990; Akitomo et al. 1991, 1997). Multiple equilibrium states are present in all these modeling studies under the intermediate inflow boundary condition. With regard to the dynamics underlying the Kuroshio path bimodality, the “consensus” from these modeling studies can be summarized as follows. When the upstream inflow transport  $V_o$  is small, the Kuroshio takes a straight path and the vorticity balance is that of the Munk-type viscous boundary layer. When  $V_o$  is large, the positive vorticity is generated along the Japan coast, which produces and maintains the presence of a downstream meandering path. In the intermediate  $V_o$  range, the transition from the meandering state to the straight-path state and vice versa are triggered by the changes in the inflow transport.

It is worth pointing out that the previous modeling studies of the Kuroshio path dynamics have all sought the correspondence between the magnitude of the inflow transport and the Kuroshio path pattern. With longer in situ observational data now available, it is possible to reassess this correspondence. In Fig. 4b, we plot, after Kawabe (1995) and M. Kawabe (1998, personal communication), the time series of the Kuroshio transport in the upstream East China Sea over the past 40 years (see Fig. 1 for the location of the repeat hydrographic section). The shaded areas indicate the large meander periods in which the Kuroshio path index shown in Fig. 4a exceeds  $1.5^\circ$ . In terms of the transport magnitude, the 1959–62 event clearly corresponds with a large inflow transport in the East China Sea. This correspondence between the path pattern and the transport magnitude becomes, however, less obvious after 1975; there are times such as 1980–81, 1986, and 1992–97 where the inflow transport was large, but no meanders were present. If we assume that the inflow Kuroshio transport after 1975 falls in the multiple equilibrium regime, previous studies have suggested that the transition from a straight path to a meander path would require an increase in inflow transport. Such an increase did occur before the events of 1975–79 and 1990, but not before the events of 1982–85 and 1987–88. In other words, the correspondence between the Kuroshio path and the magnitude and/or the temporal change of the upstream inflow transport is not conclusive based on the long-term available observational data.

One signal that stands out in the time series of Fig. 4b is the one with a decadal timescale. Specifically, the inflow transport in the upstream East China Sea prior to 1975 was low on average, whereas the mean level of the inflow transport increased after 1975. This de-

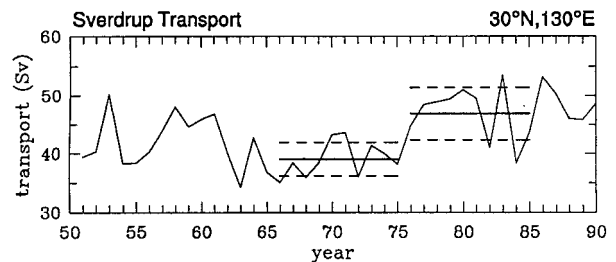


FIG. 5. Time series of the annual mean Sverdrup transport at  $30^\circ\text{N}$ ,  $130^\circ\text{E}$ . The wind stress data are based on the Comprehensive Ocean Atmosphere Data Set. Horizontal solid and dashed lines indicate means and standard deviations for 1966–75 and 1976–85, respectively. Tick marks along the time axis indicate the beginning of a year. Adapted from Yasuda and Hanawa (1997).

cadal signal in the inflow transport is a manifestation of the decadal Sverdrup transport change in the subtropical North Pacific. For example, Fig. 5 shows the time series of the annually averaged Sverdrup transport at  $30^\circ\text{N}$ ,  $130^\circ\text{E}$ , the point where one finds the largest Sverdrup transport in the subtropical North Pacific (adapted from Yasuda and Hanawa 1997). For the decade before 1975, Fig. 5 reveals that the Sverdrup transport in the subtropical North Pacific was on average low with a mean value of 39 Sv. After 1975, the Sverdrup transport jumped to a mean level of 47 Sv, a 20% increase over what was observed in the preceding decade. Comparing the Kuroshio transport in the East China Sea in the decade prior to 1975 and that since 1975 in Fig. 4b reveals a similar 20% increase (22.5 vs 27.0 Sv). For other aspects of the North Pacific decadal change in association with the 1975 climatic shift, the reader is referred to Trenberth (1990), Qiu and Joyce (1992), Miller et al. (1994), Deser and Blackmon (1995), Deser et al. (1996), and Nakamura et al. (1997).

Another point worth emphasizing is that most of the previous modeling studies on the Kuroshio path dynamics have used inflow–outflow regional models. The inflow velocity profiles were often chosen arbitrarily, including both uniform and parabolic inflow profiles. Given that the recirculation gyre is an inseparable part of the Kuroshio system as we noted above, the regional model may not be able to realistically capture the Kuroshio’s recirculation gyre whose structure depends critically on the low PV input from the southern latitude. Indeed, a recent study by Marshall and Marshall (1992) demonstrated that the intensity of the recirculation gyre depends sensitively on the velocity profile imposed at the inlet of an inflow–outflow regional model.

In light of the new observational results presented above, we decide to revisit the dynamics of the Kuroshio path bimodality from a perspective different from the previous studies. In this study, we adopt an ocean general circulation model that incorporates the realistic North Pacific coastlines and bottom topography and is driven by observed monthly climatological wind stresses. In so doing, we avoid possible dynamic effects due

to boundary condition specifications in the inflow–outflow regional model. While recognizing that the Kuroshio since 1975 is in the multiple equilibrium state, we argue that the observed oscillations between the straight and meander paths are not necessarily a result controlled deterministically by the temporal changes in the upstream Kuroshio transport. Rather, the observed alternations of the Kuroshio’s two states are proposed to be due to a self-sustained internal mechanism involving the evolution of the southern recirculation gyre and the stability of the Kuroshio current system. Different behaviors of the observed Kuroshio path changes on the decadal time scale will also be addressed in this study.

## 2. Model description

The numerical model used in this study is a two-layer primitive-equation model, in which the upper ocean of density  $\rho_1$  overlies the abyssal ocean of density  $\rho_2$ . With the interface between the two layers representing the main thermocline, this model is the dynamically simplest model that allows for baroclinic instability and the inclusion of ocean bottom topography. Both of these features are likely to be important for the Kuroshio path variability. Because of the large variations both in the thermocline tilt associated with the Kuroshio and in bottom topography and because our model domain includes the whole North Pacific basin, the primitive-equation model is more appropriate for our purpose than a model based on quasigeostrophic dynamics.

In the two-layer primitive-equation model, the governing equations can be written as follows:

$$\frac{\partial \mathbf{u}_1}{\partial t} + \mathbf{u}_1 \cdot \nabla \mathbf{u}_1 + f \mathbf{k} \times \mathbf{u}_1 = -\nabla p_s + \frac{\boldsymbol{\tau}_w}{\rho_o h_1} + w_e \frac{\mathbf{u}_2}{h_1} + A_h \nabla^2 \mathbf{u}_1, \quad (1)$$

$$\frac{\partial h_1}{\partial t} + \nabla \cdot (h_1 \mathbf{u}_1) = K_h \nabla^2 h_1 + w_e, \quad (2)$$

$$\frac{\partial \mathbf{u}_2}{\partial t} + \mathbf{u}_2 \cdot \nabla \mathbf{u}_2 + f \mathbf{k} \times \mathbf{u}_2 = -\nabla p_s + g' \nabla h_1 - w_e \frac{\mathbf{u}_2}{h_2} + A_h \nabla^2 \mathbf{u}_2, \quad (3)$$

$$\frac{\partial h_2}{\partial t} + \nabla \cdot (h_2 \mathbf{u}_2) = K_h \nabla^2 h_2 - w_e, \quad (4)$$

where  $\mathbf{u}_i$  is the  $i$ th-layer velocity vector,  $h_i$  is the  $i$ -layer thickness,  $\mathbf{k}$  is a unit vector in the vertical direction,  $A_h$  ( $K_h$ ) is the coefficient of the horizontal eddy viscosity (diffusivity),  $f$  is the Coriolis parameter,  $\boldsymbol{\tau}_w$  is the surface wind stress vector,  $\rho_o$  is the reference water density,  $g' \equiv (\rho_2 - \rho_1)g/\rho_o$  is the reduced gravity, and  $p_s$  is the surface pressure divided by  $\rho_o$ . In Eqs. (1)–(4),  $w_e$  denotes the entrainment velocity and is operative when the upper-layer thickness  $h_1$  becomes shallower than a

prescribed “entrainment depth”  $H_e$  (McCreary and Lu 1994):

$$w_e \equiv \begin{cases} (H_e - h_1)^2/t_e H_e, & h_1 \leq H_e \\ 0, & h_1 > H_e, \end{cases} \quad (5)$$

where  $t_e$  is a specified relaxation time. Following McCreary and Lu (1994), we choose  $H_e = 75$  m and  $t_e = 1$  day. For the North Pacific model adopted in this study,  $w_e$  is nonzero only in the subarctic region north of 44°N.

To minimize effects of specifying artificial boundary values, the model domain is chosen to include the Pacific Ocean from 10°S to 60°N. The model basin is bounded to the west by the Asian continent and to the east by the North and South American continents. The model has realistic coastline geometry that is determined by the 200-m depth contour. In specifying the model’s bottom topography, we used the NOAA’s ETOPO-05 dataset. The topography data was first interpolated to the model grid and smoothed thereafter with a five-point smoother. We set the maximum ocean depth at 6000 m and the minimum depth at 800 m, such that the bottom topography is confined to the lower layer of the model ocean.

Equations (1)–(5) are solved in finite difference form using the energy-conserving scheme described in Semtner (1986). As in Semtner (1986), the rigid-lid approximation is adopted. In solving the Poisson equation for the transport streamfunction, we replaced the successive over-relaxation (SOR) method by the more efficient blackbox multigrid solver developed recently by de Zeeuw (1990). Along the model’s open southern boundary, a free-slip condition is used. A no-slip condition is used along the coast or marginal seas (depth < 200 m). The model grid has the resolution of  $1/6^\circ$  by  $1/6^\circ$ . This relatively high resolution is necessary to ensure that the Kuroshio southeast of Japan separates at the observed latitude of 35°N. For a detailed discussion on how the horizontal grid resolution and other physical parameters in layered models can influence the separation of the Kuroshio, the reader is referred to Hurlburt et al. (1996). The initial upper-layer thickness of our two-layer model is 250 m and  $g' = 0.023$  m s<sup>-2</sup>. These two values are chosen such that the first-mode baroclinic Rossby waves in the model propagate at speeds similar to those determined from historical hydrographic data (e.g., Emery et al. 1984) and that the modeled upper-layer thickness matches the observed 26.4  $\sigma_\theta$  surface. The 26.4  $\sigma_\theta$  surface lies at the base of the ventilated thermocline of the North Pacific (e.g., Huang and Qiu 1994). The horizontal eddy viscosity and diffusivity coefficients in the model are  $A_h = 800$  m<sup>2</sup> s<sup>-1</sup> and  $K_h = 80$  m<sup>2</sup> s<sup>-1</sup>, respectively.

The model ocean is initialized at rest and spun up by the monthly climatological wind of Hellerman and Rosenstein (1983). It reached a statistical steady state after 30 years of time integration. After the spinup, we in-

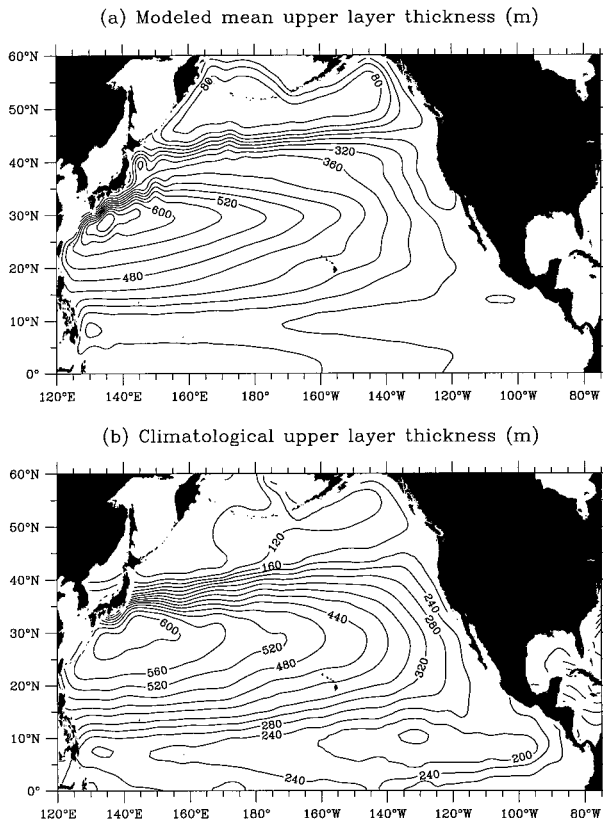


FIG. 6. (a) Mean upper-layer thickness field from the long-term model integration. (b) Depth of the  $26.4 \sigma_\theta$  surface based on the climatological dataset of Levitus and Boyer (1994) and Levitus et al. (1994).

tegrated the model for an additional 36 years and the model results from these years are used in the following analyses. In addition to this base model case, we ran a case in which we reduced the magnitude of the Hellerman and Rosenstein wind stress by 25% (see section 4). The initial condition for this reduced wind case is the 30th-year state of the base model case.

### 3. Model results and analysis

#### a. Large-scale mean circulation

Before discussing the Kuroshio path variability, we note that the two-layer primitive-equation model described in section 2 adequately simulates the basin-scale, wind-driven circulation pattern of the North Pacific. Figure 6 compares the mean upper-layer thickness field derived from the model to the depth of the  $26.4 \sigma_\theta$  surface computed from the climatological datasets of Levitus and Boyer (1994) and Levitus et al. (1994). In both the model and the observations, the westward-flowing North Equatorial Current is found to bifurcate at  $14^\circ\text{N}$  along the western boundary with its northern branch forming the Kuroshio. Offshore of the Kuroshio south of Japan, both Figs. 6a and 6b show the presence of the southern re-

circulation gyre near the same geographical location. In the subpolar gyre north of  $40^\circ\text{N}$ , the  $26.4 \sigma_\theta$  surface is close to the base of the winter mixed layer. As a result, it is subject to the surface buoyancy forcing that is absent in our present model. For the wind-driven circulation in the subpolar gyre, a more meaningful comparison is between Fig. 6a and the sea surface dynamic height field shown in Fig. 1.<sup>1</sup> As in Fig. 1, Fig. 6a shows that the subpolar circulation in the North Pacific consists of two subgyres, the Alaskan gyre east of  $170^\circ\text{W}$  and the western subarctic gyre west of  $170^\circ\text{W}$ . Both figures show that the western subarctic gyre extends northward into the deep basin of the Bering Sea.

Discrepancies between the model and the observations exist as well. In the Kuroshio Extension east of Japan, while the main body of the modeled Kuroshio Extension flows eastward as in the observations, Fig. 6a shows that a branch of it curves northward and joins the eastward flow of the Subarctic Front along  $42^\circ\text{N}$ . This northward branch is not an observed feature of the Kuroshio Extension and is due to the fact that the east-northeastward penetration of the modeled Kuroshio Extension is too weak. This deficiency is likely due to the grid resolution used in our present model ( $1/6^\circ \times 1/6^\circ$ ). A recent study by Hurlburt et al. (1996) indicates that the simulation of a realistic zonal penetration of the Kuroshio Extension requires a grid resolution as high as  $1/16^\circ$ . When the grid spacing is reduced from  $1/8^\circ$  to  $1/16^\circ$  while keeping other model parameters the same, Hurlburt et al. show that the Kuroshio Extension remains a narrow inertial jet beyond the Shatsky Rise and that the eddy kinetic energy level associated with the meandering jet compares much more favorably with observations. Despite this problem of our modeled Kuroshio Extension, we believe that the large-scale gyre circulation of the North Pacific is adequately simulated and that the model captures the essential features of the Kuroshio system in the region south of Japan.

#### b. Modeled Kuroshio path bimodality

To examine the time-varying features of the Kuroshio south of Japan, we plot in Fig. 7 the Kuroshio path index from the multiyear model output. As in Fig. 4a, the Kuroshio path index is defined as the distance of the Kuroshio axis from the Japan coast averaged from  $132^\circ$  to  $140^\circ\text{E}$ . Despite the climatological wind forcing, Fig. 7 shows that the modeled Kuroshio path variability is dominated by interannual changes. A spectral analysis shows that the path oscillation has a preferred timescale of 4.0 yr, although individual events are highly chaotic. For example, in both model years 42 and 61, the Kuroshio shifted to the meandering state and stayed in this

<sup>1</sup> Under the two-layer approximation, the modeled upper-layer thickness contours can be regarded as streamlines of the surface-layer flow.

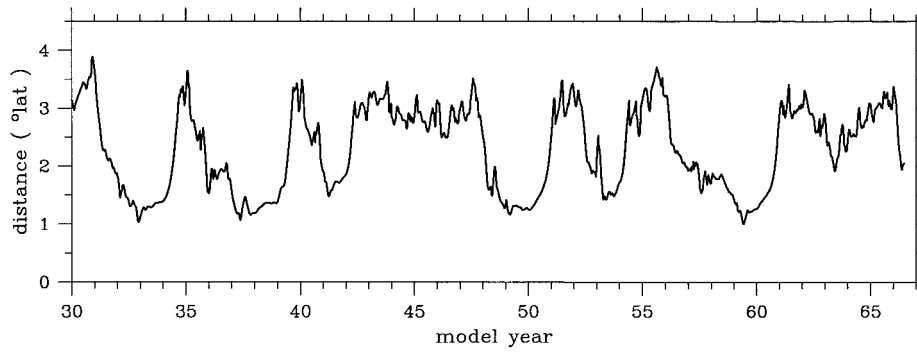


FIG. 7. Time series of the Kuroshio path index from the two-layer primitive-equation model. The model is driven by the monthly, climatological wind stress data of Hellerman and Rosenstein (1983). The Kuroshio path index is defined here as the mean distance of the Kuroshio axis from the Japan coast (132°–140°E). Tick marks along the time axis indicate the beginning of a year.

state for the consecutive 5 years. Notice that as in the observations, transitions between the two path states in the model take place in a relatively short time period (i.e., <1 yr).

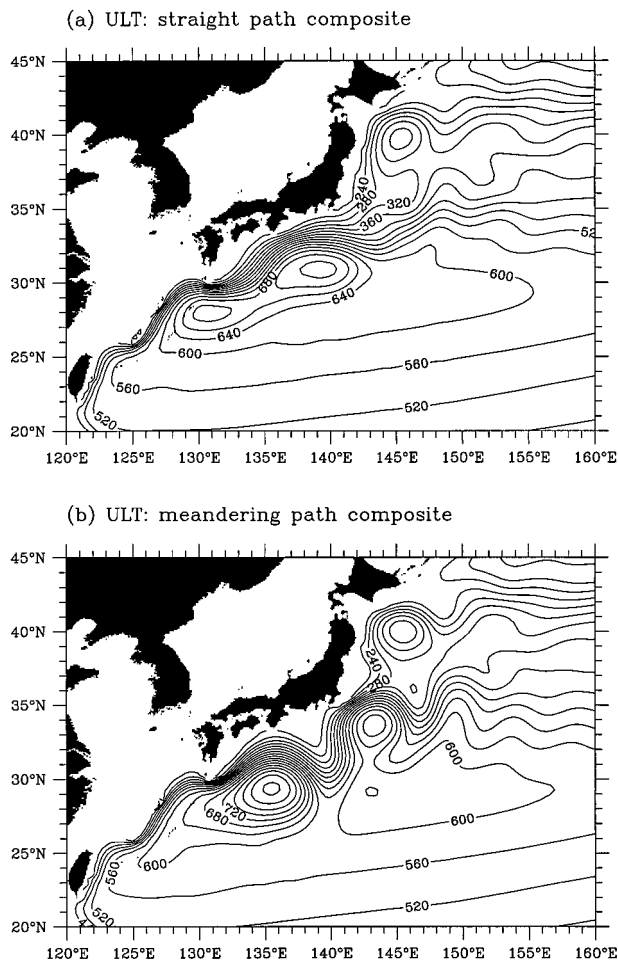


FIG. 8. Composite upper-layer thickness field for (a) the straight path years and (b) the meander path years.

Figures 8a and 8b show the upper-layer thickness fields composited from the straight path years (the Kuroshio path index < 1.8°) and the meander path years (the Kuroshio path index > 2.5°), respectively. It is interesting to note that the two states of the simulated Kuroshio paths bear close resemblance to the observed bimodal Kuroshio paths presented in Fig. 3. To provide a general idea of how the modeled Kuroshio path evolves, we plot in Fig. 9 a sequence of the upper-layer thickness field encompassing the meander event of year 34–35 (see Fig. 7). Figure 9a shows the Kuroshio in its typical straight path state prior to the meander development. Figure 9b shows that a meander emerges in the Kuroshio path. This meander grows steadily in amplitude in subsequent months (Figs. 9c and 9d) and it eventually breaks off to form an isolated cold-core eddy (Fig. 9e). Figure 9f shows that this detached cold-core eddy drifts westward and a new meander starts to develop. This meander sheds the second cold-core eddy after its amplitude fully grows (Fig. 9g). Following the detachment of this second cold-core eddy, the Kuroshio path returns to the low-path-index state (Fig. 9h).

It is worth mentioning that similar detachments of isolated cold-core eddies from fully developed Kuroshio meanders were detected in in situ observations. Figure 10 shows three such cases during the Kuroshio's 1975–79 meander event reported by Nishida (1982). In all these cases, the meandering Kuroshio path was observed to become meridionally elongated prior to the break-off of the cold-core eddies. According to Nishida (1982), the cold-core eddy of May 1977 (Fig. 10a) moved northwestward in the subsequent two months and was absorbed later by a newly formed upstream meander. The detachment of the cold-core eddy in August 1979 (Fig. 10c), on the other hand, signaled the end of the 1975–79 meander event. As will be discussed in section 4, the detachment of these cold-core eddies carries coast-originated high-PV water offshoreward and is important in the regulation of the modeled path oscillations.

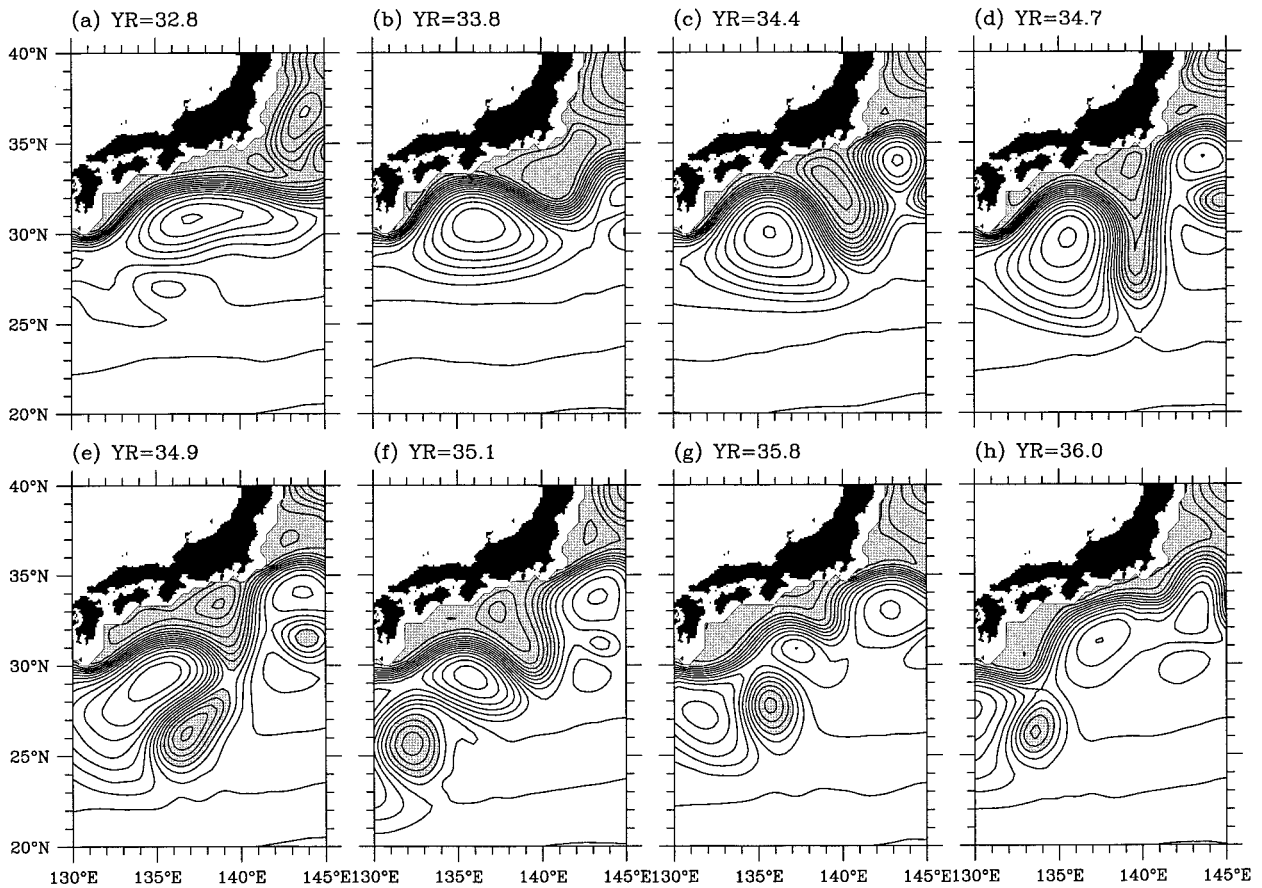


FIG. 9. Sequence of the upper-layer thickness ( $h_1$ ) field encompassing the meander event around model year 35 (Fig. 7). The contour interval for the thickness field is 50 m and regions with  $h_1 < 350$  m are stippled.

### c. Path fluctuations versus instability

A useful tool for gaining a better understanding of the variability of oceanic flows is analysis of energetics. Given the spatial and temporal inhomogeneity of the circulation, an ideal way of examining the Kuroshio path fluctuations is to look into the conversions between the mean and eddy potential energies ( $\bar{P}$  and  $P'$ ) and between the mean and eddy kinetic energies ( $\bar{K}$  and  $K'$ ) in a boxed region south of Japan. In the two-layer primitive equation model, the conversion rate between  $\bar{P}$  and  $P'$ , for example, is simply

$$\{\bar{P}, P'\} = -\rho_0 g' \langle \overline{h'_1 \mathbf{u}'_1} \cdot \nabla \bar{h}_1 \rangle, \quad (6)$$

(see Holland and Lin 1975) where overbars denote time averages, primes denote deviations from the time average, and angle brackets denote the spatial average. For an open boxed region, unfortunately, the conversion rates, such as the one defined in Eq. (6), do not discriminate between energy conversions and the energy fluxes through the open boundaries (Harrison and Robinson 1978). For the Kuroshio region south of Japan, say from 25° to 35°N, 132° to 140°E, the eddy energy fluxes through the open eastern boundary are substantial (see Fig. 9).

Because of this ambiguity in interpreting the energy conversion rates for the regional energy budget, we will instead examine the lower-layer kinetic energy ( $K_2$ ) in a region south of Japan. Previous studies by Holland and Lin (1975) and Holland and Haidvogel (1981) show that barotropic and baroclinic instability in the two-layer ocean models is characterized by a sharp rise in  $K_2$  and a drop in  $K_1$  (the upper-layer kinetic energy) following the instability.<sup>2</sup> Physically, the rise in the lower-layer kinetic energy is due to the downward momentum transfer resulting from baroclinic instability. Figure 11 shows the time series of  $K_2$  averaged in the box south of Japan (25°–35°N, 132°–140°E). Notice that though open, this box is effectively isolated to the east due to the presence of Izu Ridge. In other words, the  $K_2$  changes seen in Fig. 11 largely reflects the vertical energy transfers due to instability.

Comparing the  $K_2$  time series with that of the Kuroshio path index (Fig. 7) reveals that the transition in

<sup>2</sup> In both of these studies, the model domain is small and the energy conversion rates, calculated in the closed model domain, can be uniquely interpreted.

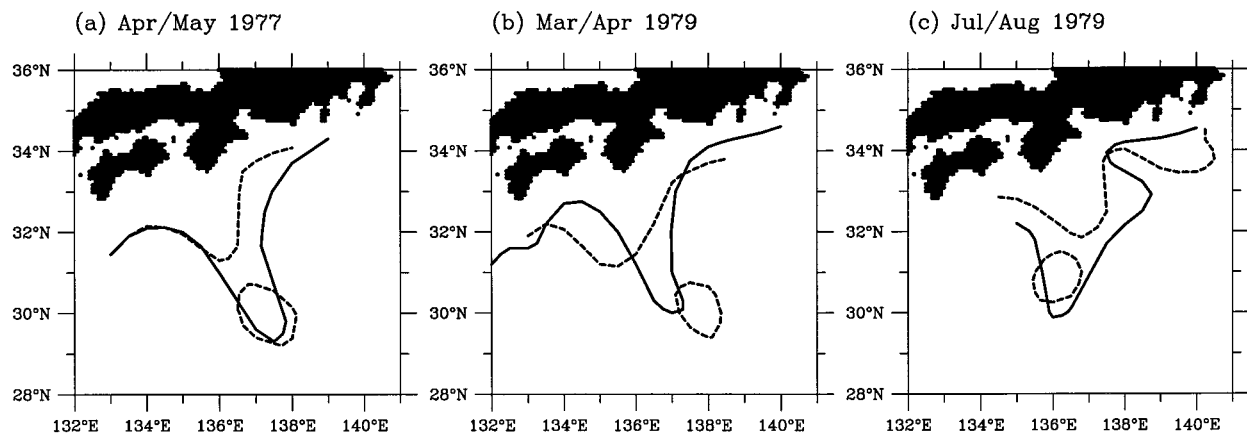


FIG. 10. Examples of the observed cold-core eddy detachment from fully-developed Kuroshio meanders. (a) 20–30 Apr (solid line) vs 20–30 May (dashed lines) 1977; (b) 3–15 Mar vs 28 Mar–9 Apr 1979; (c) 18 Jul–1 Aug vs 8–23 Aug 1979. Redrawn from Nishida (1982).

the Kuroshio from a straight path state to a meandering state is nearly always accompanied by a sharp rise in  $K_2$ . From the studies of Holland and colleagues, this implies that the development of the Kuroshio meanders is preceded by the occurrence of baroclinic instability. That the baroclinic instability takes place at a late stage of the Kuroshio's straight path state is also supported by signals seen in the vertical shear of the alongshore Kuroshio,  $\langle U_1 - U_2 \rangle$ , where  $U_i = u_i \cos 23^\circ + v_i \sin 23^\circ$  denotes the flow speed parallel to the Japan coast. As shown in Fig. 12a, the mean vertical shear of the Kuroshio south of Japan undergoes a gradual buildup while the Kuroshio is in its straight path state. It is likely that the straight-pathed Kuroshio eventually becomes baroclinically unstable when  $\langle U_1 - U_2 \rangle$  exceeds a threshold value.

What, then, causes the gradual increase in  $\langle U_1 - U_2 \rangle$  when the Kuroshio is in the straight path state? As we noted in the introduction, the eastward flow of the Kuroshio is closely connected to the anticyclonic recirculation gyre to its south. Many theoretical and modeling studies in the past have shown that the southern

recirculation gyre in the wind-driven subtropical circulation is due to the accumulation of low-PV anomalies carried northward by the western boundary current (e.g., Cessi et al. 1987; Ireley and Young 1988; Böning 1986; Spall 1996a,b; and Liu 1997). The equilibrium state of the recirculation gyre, as shown in these studies, depends on the magnitude of the low-PV anomalies transported by the western boundary current and the size of subgrid-scale eddy dissipation. When the latter is insufficient to offset the low-PV anomalies, the recirculation gyre will increase in intensity and the dispersal of the excessive low-PV anomalies is accomplished through the flow instability. We believe that our modeled Kuroshio is in such a parameter regime where the low-PV anomalies transported from the south are not being effectively removed from the region south of Japan. Indeed, a look into the upper-layer vorticity  $\langle \zeta_1 \rangle$  in the region south of Japan reveals that when the Kuroshio is in the straight path state, the area-averaged  $\langle \zeta_1 \rangle$  has in general a *decreasing trend*, indicating a regional accumulation of the low-PV anomalies (see Fig. 12b). The low-PV anomaly accumulation spins up the anticyclonic

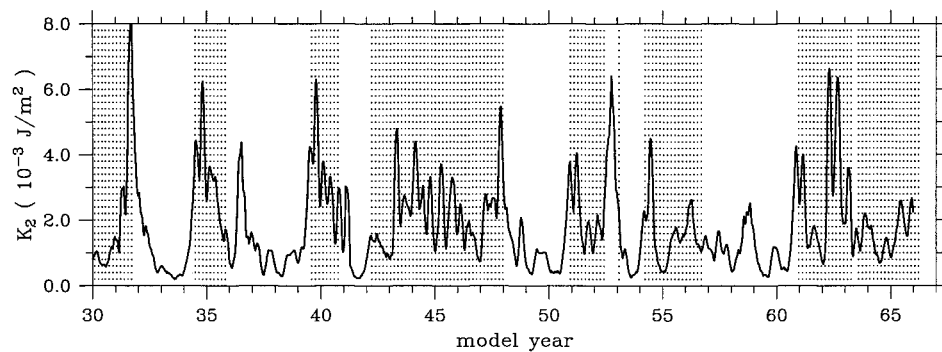


FIG. 11. Time series of the lower-layer kinetic energy,  $K_2 = \rho_0 h_2 (u_2^2 + v_2^2)/2$ , averaged in the Kuroshio region south of Japan ( $25^\circ$ – $35^\circ$ N,  $132^\circ$ – $140^\circ$ E). Shaded periods indicate when the Kuroshio is in the meandering state (i.e., the Kuroshio path index in Fig. 7  $> 2.0^\circ$ ). Tick marks along the time axis indicate the beginning of a year.

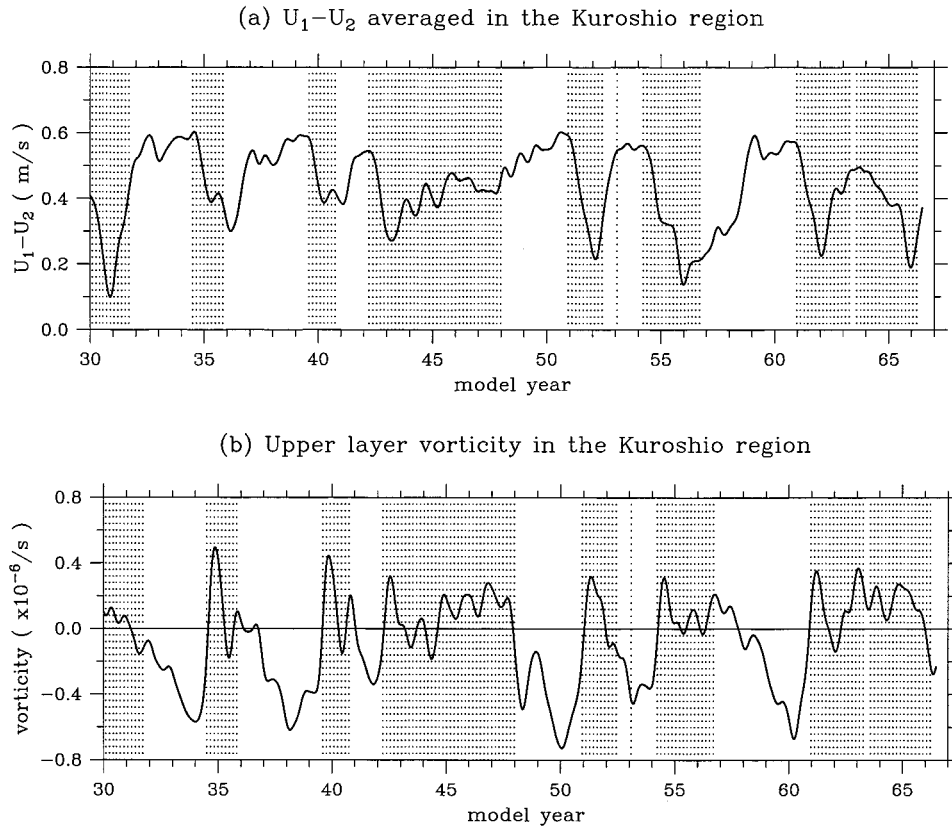


FIG. 12. (a) Time series of the vertical shear in the alongshore Kuroshio current,  $\langle U_1 - U_2 \rangle$ , where  $\langle \rangle$  denotes the spatial average in the area from  $132^\circ$  to  $140^\circ\text{E}$  and from  $0.5^\circ$  to  $3.5^\circ$  offshore from the Japan coast. (b) Time series of the upper layer vorticity  $\zeta_1$ , averaged in the Kuroshio region of  $25^\circ$ – $35^\circ\text{N}$  and  $132^\circ$ – $140^\circ\text{E}$ . For both time series, a low-pass Gaussian filter with an  $e$ -folding scale of 80 days was applied to remove high-frequency signals. Shaded periods indicate when the Kuroshio is in the meandering state (i.e., the Kuroshio path index in Fig. 7  $> 2.0^\circ$ ). Tick marks along the time axes indicate the beginning of a year.

recirculation gyre and increases the eastward flow in the upper-layer Kuroshio. With the vertical shear increases in the alongshore Kuroshio, this leads eventually to baroclinic instability of the straight-pathed Kuroshio system.

#### 4. Discussion and conclusions

The notion that the Kuroshio path modality could be a result of multiple equilibrium states has been recognized by many previous theoretical and modeling studies. As we reviewed in the introduction, when the Kuroshio is in the multiple equilibrium regime, the existing studies have emphasized the importance of inflow changes in determining the path transitions from one state to the other. In other words, the Kuroshio path variability has been considered a hysteresis phenomenon controlled externally by the upstream inflow fluctuations and dependent on the history of the existing path.

The result of this study indicates that the Kuroshio's bimodal path fluctuations are not necessarily regulated by the external inflow changes. It suggests the existence of a self-sustained mechanism in the Kuroshio current

system that can generate bimodal path variations on an interannual time scale. This mechanism can be briefly summarized as follows (Fig. 13). Being the western boundary current for the subtropical circulation of the North Pacific, the Kuroshio carries northward low-PV water of southern origin. In the “reentry” region south of Japan, the inability of dissipative processes to remove the low-PV anomalies intensifies the offshore recirculation gyre, forcing the Kuroshio to flow along the Japan coast. As the intensification of the recirculation gyre progresses, the vertical velocity shear of the Kuroshio increases, leading eventually to the development of a meander path due to baroclinic instability of the straight-pathed Kuroshio. Through shedding of cyclonic cold-core eddies offshoreward, the meandering Kuroshio mixes high-PV water of coastal origin into the recirculation gyre, thereby reducing the intensity of the anticyclonic recirculation gyre. Once the Kuroshio is in its meandering state, its return to the succeeding straight path state has to wait for the re-strengthening of the offshore recirculation gyre. The restrengthening of the recirculation gyre is a slow process; it depends on the gradual accumulation of low-PV anomalies replenished

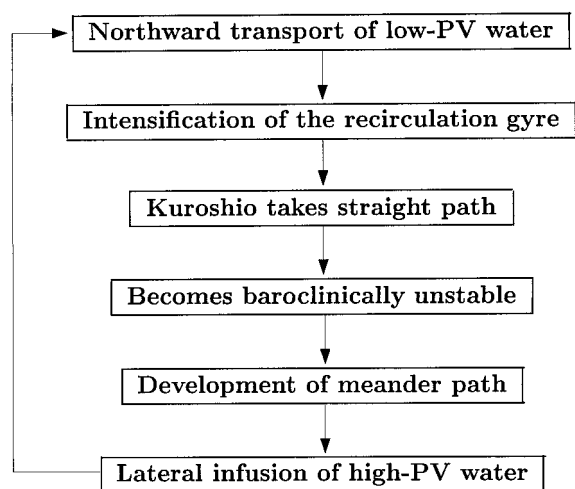


FIG. 13. Schematic of the self-sustained oscillation mechanism of the Kuroshio current system.

by the upstream Kuroshio in excess of eddy dissipation. After the recirculation gyre intensifies, the cycle described above would start again.

On the interannual timescale, we note that the observed Kuroshio transport in the upstream East China Sea has remained at a relatively constant level since 1975 (Fig. 4b). Given the weak correspondence between the changes in the upstream inflow and in the Kuroshio path, we suggest that the observed alternations of the Kuroshio path following 1975 (Fig. 4a) may be better understood as a manifestation of the above self-sustained oscillation. Because many of the dynamical processes listed in Fig. 13 are strongly nonlinear, the oscillation is likely to recur aperiodically. Indeed, the modeled Kuroshio path index of Fig. 7 showed that the duration of the meander state and the time interval between the two consecutive meander states varied from event to event.

While quantifying the explicit dependence of the oscillation timescale upon the upstream Kuroshio transport is beyond the scope of this study, we did carry out one additional model run in which we reduced the surface wind stress forcing over the entire model domain by 25% after model year 30. In this reduced wind forcing case, the mean Sverdrup transport evaluated at 30°N and 130°E is 40 Sv, the level corresponding to that observed in the decade from 1965 to 1974 as shown in Fig. 5. The solid line in Fig. 14 shows the Kuroshio path index obtained from this model case. While small-amplitude path fluctuations are abundant, the Kuroshio remains in the straight path state after the initial period of adjustment. This model result can again be explained by the dynamics of the southern recirculation gyre. When the basinwide surface wind forcing is weak, the upstream Kuroshio inflow becomes small. If the dissipative forces south of Japan are sufficient to remove the excess low-PV anomalies transported from the south,

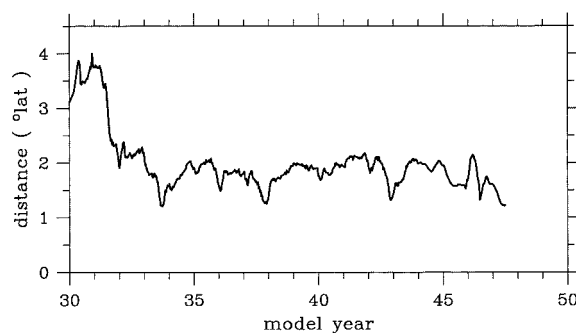


FIG. 14. Time series of the Kuroshio path index from the model driven by the monthly Hellerman and Rosenstein wind stress data at the 75% level. The initial condition for this reduced wind forcing case is the 30th-year state of the base model case. Tick marks along the time axis indicate the beginning of a year.

the Kuroshio will remain in the straight path state without instability and meander development. As such, the relatively weak surface wind forcing over the North Pacific Ocean during the decade of 1965–74 likely explains why the Kuroshio remained in a straight path state for the long ten-year period before 1975 (Fig. 4a).

In the self-sustained oscillation proposed above, we emphasized the dynamic role played by the Kuroshio's southern recirculation gyre. The importance of recirculation gyres in contributing to the multiple equilibrium states of a western boundary outflow has been the subject of several recent studies (e.g., Jiang et al. 1995; McCalpin and Haidvogel 1996; Spall 1996a,b). In particular, Spall's (1996a,b) study identified a decadal-timescale internal oscillation in the Gulf Stream, as a result of the Gulf Stream's interaction with the underlying deep western boundary current. In his model, the Gulf Stream switches back and forth between a low energy state with weak northern/southern recirculation gyres and short penetration scale and a high energy state with stronger recirculation gyres and longer penetration scale. As in Fig. 13, the Gulf Stream oscillation is maintained by the spinup and spindown of the recirculation gyres and by variations in the stability property of the surface boundary outflow. The contributing processes of the oscillations are, however, different. For example, the Gulf Stream oscillation depends critically on the presence of the deep western boundary current, which supplies low-PV water to the southern recirculation gyre when the Gulf Stream is in the high energy state, subtly changing the stability property of the Gulf Stream. For the Kuroshio, the low-PV water supply is solely from the upstream upper-layer inflow. Of fundamental importance for the Kuroshio path oscillation is the presence of the Japan coast acting as a solid northern wall. The wall prohibits the formation of a northern recirculation gyre as in the Gulf Stream (Hogg et al. 1986), and confines the Kuroshio in a straight path state when the southern recirculation gyre spins up.

The two-layer model is admittedly an over-simplified

representation of the Kuroshio current system. No attempt is made in this study to simulate the observed Kuroshio path index time series (Fig. 4a) by using available interannually varying wind stress data. It is our hope that the results from this study provide insight into the dynamical processes crucial for the Kuroshio path bimodality that can be further explored in future observational and modeling studies.

*Acknowledgments.* This study benefited from discussions with Drs. Michael Ghil, Peter Hacker, and Humio Mitsudera. Detailed comments made by the two anonymous reviewers helped clarify many parts of an early version of the manuscript. The PN-Line Kuroshio transport time series presented in Fig. 4b was generously provided to us by Dr. Masaki Kawabe. Dr. Paul de Zeeuw generously provided us with the blackbox multigrid solver used in our modeling work. Support from NASA through the Young Investigators Award NAGW-5250 and from NSF through Grant OCE99-11268 is gratefully acknowledged.

## REFERENCES

- Akitomo, K., T. Awaji, and N. Imasato, 1991: Kuroshio path variation south of Japan I. Barotropic inflow-outflow model. *J. Geophys. Res.*, **96**, 2549–2560.
- , S. Masuda, and T. Awaji, 1997: Kuroshio path variation south of Japan: Stability of the paths in a multiple equilibrium regime. *J. Oceanogr.*, **53**, 129–142.
- Böning, C. W., 1986: On the influence of frictional parameterization in wind-driven circulation models. *Dyn. Atmos. Oceans*, **10**, 63–92.
- Cessi, P., G. Ierley, and W. Young, 1987: A model of the inertial recirculation driven by potential vorticity anomalies. *J. Phys. Oceanogr.*, **17**, 1640–1652.
- , R. V. Condie, and W. Young, 1990: Dissipative dynamics of western boundary currents. *J. Mar. Res.*, **48**, 677–700.
- Chao, S. Y., 1984: Bimodality of the Kuroshio. *J. Phys. Oceanogr.*, **14**, 92–103.
- , and J. P. McCreary, 1982: A numerical study of the Kuroshio south of Japan. *J. Phys. Oceanogr.*, **12**, 679–693.
- Deser, C., and M. L. Blackmon, 1995: On the relationship between tropical and North Pacific sea surface variations. *J. Climate*, **8**, 1677–1680.
- , M. A. Alexander, and M. S. Timlin, 1996: Upper-ocean thermal variations in the North Pacific during 1970–91. *J. Climate*, **9**, 1840–1855.
- de Zeeuw, P. M., 1990: Matrix-dependent prolongations and restrictions in a blackbox multigrid solver. *J. Comput. Appl. Math.*, **33**, 1–27.
- Emery, W. J., W. G. Lee, and L. Magaard, 1984: Geographical and seasonal distributions of Brunt-Väisälä frequency and Rossby radii in the North Pacific and North Atlantic. *J. Phys. Oceanogr.*, **14**, 294–317.
- Firing, E., 1998: Lowered ADCP development and use in WOCE. *Int. WOCE Newslett.*, **30**, 10–14.
- Harrison, D. E., and A. R. Robinson, 1978: Energy analysis of open regions of turbulent flows—Mean eddy energetics of a numerical ocean circulation experiment. *Dyn. Atmos. Oceans*, **2**, 185–211.
- Hautala, S. L., D. H. Roemmich, and W. J. Schmitz Jr., 1994: Is the North Pacific in Sverdrup balance along 24°N? *J. Geophys. Res.*, **99**, 16 041–16 052.
- Hellerman, S., and M. Rosenstein, 1983: Normal monthly wind stress over the world ocean with error estimates. *J. Phys. Oceanogr.*, **13**, 1093–1104.
- Hogg, N. G., R. S. Pickart, R. M. Hendry, and W. J. Smethie Jr., 1986: The northern recirculation gyre of the Gulf Stream. *Deep-Sea Res.*, **33**, 1139–1165.
- Holland, W. R., and L. B. Lin, 1975: On the generation of mesoscale eddies and their contribution to the oceanic general circulation. I. A preliminary numerical experiment. *J. Phys. Oceanogr.*, **5**, 642–657.
- , and D. B. Haidvogel, 1981: On the vacillation of an unstable baroclinic wave field in an eddy-resolving model of the oceanic circulation. *J. Phys. Oceanogr.*, **11**, 557–568.
- Huang, R. X., and B. Qiu, 1994: Three-dimensional structure of the wind-driven circulation in the subtropical North Pacific. *J. Phys. Oceanogr.*, **24**, 1608–1622.
- Hurlburt, H. E., A. J. Wallcraft, W. J. Schmitz, P. J. Hogan, and E. J. Metzger, 1996: Dynamics of the Kuroshio/Oyashio current system using eddy-resolving models of the North Pacific Ocean. *J. Geophys. Res.*, **101**, 941–976.
- Ierley, G. R., and W. R. Young, 1988: Inertial recirculation in a  $\beta$ -plane corner. *J. Phys. Oceanogr.*, **18**, 683–689.
- Japan Marine Safety Agency, 1955–79: *State of the Adjacent Seas of Japan*. Vols. 1–5, Marine Safety Agency, Tokyo, Japan.
- , 1977–85: *Oceanographic Atlas of Kuroshio Exploration and Utilization Research*. Vols. 1–9, Marine Safety Agency, Tokyo, Japan.
- , 1986–92: *Oceanographic Atlas of Japan-China Joint Research Program on the Kuroshio*. Vols. 1–7, Marine Safety Agency, Tokyo, Japan.
- , 1993–97: *Prompt Reports on Oceanographic Condition*. Marine Safety Agency, Tokyo, Japan.
- Jiang, S., F. F. Jin, and M. Ghil, 1995: Multiple equilibria, periodic, and aperiodic solutions in a wind-driven, double-gyre, shallow-water model. *J. Phys. Oceanogr.*, **25**, 764–786.
- Kawabe, M., 1980: Sea level variations around the Nansei Islands and the large meander in the Kuroshio south of central Japan. *J. Oceanogr. Soc. Japan*, **36**, 227–235.
- , 1985: Sea level variations at the Izu Islands and typical stable paths of the Kuroshio. *J. Oceanogr. Soc. Japan*, **41**, 307–326.
- , 1986: Transition processes between the three typical paths of the Kuroshio. *J. Oceanogr. Soc. Japan*, **42**, 174–191.
- , 1995: Variations of current path, velocity, and volume transport of the Kuroshio in relation with the large meander. *J. Phys. Oceanogr.*, **25**, 3103–3117.
- Kawai, H., 1969: Statistical estimation of isotherms indicative of the Kuroshio axis. *Deep-Sea Res.*, **16**, 109–115.
- Levitus, S., and T. Boyer, 1994: *World Ocean Atlas 1994*. Vol. 4: *Temperature*, NOAA Atlas NESDIS 4, U.S. Govt. Printing Office, 117 pp.
- , R. Burgett, and T. Boyer, 1994: *World Ocean Atlas 1994*. Vol. 3, *Salinity*, NOAA Atlas NESDIS 3, U.S. Govt. Printing Office, 99 pp.
- Liu, Z., 1997: The influence of stratification on the inertial recirculation. *J. Phys. Oceanogr.*, **27**, 926–940.
- Marshall, D., and J. Marshall, 1992: Zonal penetration scale of mid-latitude oceanic jets. *J. Phys. Oceanogr.*, **22**, 1018–1032.
- Masuda, A., 1982: An interpretation of the bimodal character of the stable Kuroshio path. *Deep-Sea Res.*, **29**, 471–484.
- McCalpin, J. D., and D. B. Haidvogel, 1996: Phenomenology of the low-frequency variability in a reduced-gravity, quasigeostrophic double-gyre model. *J. Phys. Oceanogr.*, **26**, 739–752.
- McCreary, J. P., and P. Lu, 1994: On the interaction between the subtropical and the equatorial oceans: The subtropical cell. *J. Phys. Oceanogr.*, **24**, 466–497.
- Miller, A. J., D. R. Cayan, T. P. Barnett, N. E. Graham, and J. M. Oberhuber, 1994: Interdecadal variability of the Pacific Ocean: Model response to observed heat flux and wind stress anomalies. *Climate Dyn.*, **9**, 287–302.
- Nakamura, H., G. Lin, and T. Yamagata, 1997: Decadal climate var-

- iability in the North Pacific during the recent decades. *Bull. Amer. Meteor. Soc.*, **78**, 2215–2225.
- Nishida, H., 1982: Description of the Kuroshio meander in 1975–1980—Large meander of the Kuroshio in 1975–1980. *Rep. Hydrogr. Res.*, **17**, 181–207.
- Nitani, H., 1975: Variation of the Kuroshio south of Japan. *J. Oceanogr. Soc. Japan*, **31**, 154–173.
- Pedlosky, J., 1987: *Geophysical Fluid Dynamics*. Springer-Verlag, 710 pp.
- Qiu, B., and T. M. Joyce, 1992: Interannual variability in the mid- and low-latitude western North Pacific. *J. Phys. Oceanogr.*, **22**, 1062–1079.
- Saiki, M., 1982: Relation between the geostrophic flux of the Kuroshio in the eastern China Sea and its large meanders in south of Japan. *Oceanogr. Mag.*, **32**, 11–18.
- Sekine, Y., 1990: A numerical experiment on the path dynamics of the Kuroshio with reference to the formation of the large meander path south of Japan. *Deep-Sea Res.*, **37**, 359–380.
- Semtner, A. J., Jr., 1986: Finite-difference formulation of a world ocean model. *Advanced Physical Oceanographic Numerical Modelling*, J. J. O'Brien, Ed., D. Reidel, 187–202.
- Shoji, D., 1972: Time variation of the Kuroshio south of Japan. *Kuroshio—Its Physical Aspects*, H. Stommel and K. Yoshida, Eds., University of Tokyo Press, 217–234.
- Spall, M. A., 1996a: Dynamics of the Gulf Stream/deep western boundary current crossover. Part I: Entrainment and recirculation. *J. Phys. Oceanogr.*, **26**, 2152–2168.
- , 1996b: Dynamics of the Gulf Stream/deep western boundary current crossover. Part II: Low-frequency internal oscillations. *J. Phys. Oceanogr.*, **26**, 2169–2182.
- Taft, B. A., 1972: Characteristics of the flow of the Kuroshio south of Japan. *Kuroshio—Its Physical Aspects*, H. Stommel and K. Yoshida, Eds., University of Tokyo Press, 165–216.
- Trenberth, K. E., 1990: Recent observed interdecadal climate changes in the Northern Hemisphere. *Bull. Amer. Meteor. Soc.*, **71**, 988–993.
- White, W. B., and J. P. McCreary, 1976: On the formation of the Kuroshio meander and its relationship to the large-scale ocean circulation. *Deep-Sea Res.*, **23**, 33–47.
- Wijffels, S. E., M. M. Hall, T. Joyce, D. J. Torres, P. Hacker, and E. Firing, 1998: Multiple deep gyres of the western North Pacific: A WOCE section along 149°E. *J. Geophys. Res.*, **103**, 12 985–13 009.
- Wyrtki, K., L. Magaard, and J. Hagar, 1976: Eddy energy in the ocean. *J. Geophys. Res.*, **81**, 2641–2646.
- Yamagata, T., and S. I. Umatani, 1989: Geometry-forced coherent structures as a model of the Kuroshio large meander. *J. Phys. Oceanogr.*, **19**, 130–139.
- Yasuda, I., J. H. Yoon, and N. Sugimotohara, 1985: Dynamics of the Kuroshio large meander—Barotropic model. *J. Oceanogr. Soc. Japan*, **41**, 259–273.
- Yasuda, T., and K. Hanawa, 1997: Decadal changes in the mode waters in the midlatitude North Pacific. *J. Phys. Oceanogr.*, **27**, 858–870.
- Yoon, J. H., and I. Yasuda, 1987: Dynamics of the Kuroshio large meander: Two-layer model. *J. Phys. Oceanogr.*, **17**, 66–81.